Geochemical Perspectives Letters

Fluid discharge linked to bending of the incoming plate at the Mariana subduction zone

M. Du, X. Peng, W.E. Seyfried Jr., K. Ta, Z. Guo, S. Chen, I.-M. Chou, J. Li, H. Xu

Supplementary Information

The Supplementary Information includes:

- Materials and Methods
- Supplementary Text
- Tables S-1 to S-6
- Figures S-1 and S-8
- Video S-1
- Supplementary Information References

Materials and Methods

Chemical compositions of iddingsite and augite

Electron probe microanalysis (EPMA) was performed on polished thin sections to obtain chemical compositions of iddingsite and augite (Table S-2) using the JEOL JXA-8230 at Tongji University. All quantitative analyses were performed with a combination of silicate and oxide standards as well as apatite for P. Measurements were conducted under the conditions with 15 kV acceleration voltage, 1-5 μm beam diameter, and 10 nA beam current on a probe current detector to minimise beam damage experienced by iddingsite which may contain volatiles.

Micro-Raman spectra of iddingsite and augite

Micro-Raman spectroscopy was performed for augite and iddingsite using a LabRAM HR Evolution (Horiba Jobin Yvon) Raman spectrometer at Institute of Deep-sea Science and Engineering, Chinese Academy of Sciences (Fig. S-2). Measurements were conducted under the conditions with 50 × objective lens, ~1 μm diameter analysing spot area, 532 nm excitation laser, and 10 s × 2 measuring sequence. Two laser powers, ~ 3 mW and ~1 mW, were selected for augite and iddingsite, respectively.

Whole-rock major element compositions of rocks

Rock samples were collected by the manipulator of the manned submersible *Jiaolong*. Major elements of rocks (Table S-3) were measured using a Shimadzu XRF-1800 X-ray fluorescence spectrometer (XRF) operated at 40 kV and 95 mA at Shanghai University after the fusion of 0.1 g of sample material with 3.6 g of dilithium tetraborate at 1050 °C for 16 min.

X-ray diffraction (XRD)

Mineral compositions were determined using Cu Kα radiation on a Bruker D8 Advance X-ray diffractometer (XRD), which was operated at 40 kV and 40 mA with a scanning speed of 2°/min between 3° and 70° at Guangzhou Institute of Geochemistry, Chinese Academy of Sciences. Prior to analysis, small pieces of the analysed rocks were ultrasonicated in deionised water, freeze-dried under anoxic conditions to avoid oxidation during drying and then thoroughly ground using a pestle and mortar.

Characterisation of pore water chemistry

Samples for cations (Na^+, K^+, Ca^{2+}, Mg^{2+}) and anions (Cl^-, SO_4^{2-}) in pore-water were diluted 100 times and analysed using a Thermo ICS900 ion chromatograph equipped with a Dionex IonPac CS12A and Dionex IonPac AS19, respectively, at Institute of Deep-sea Science and Engineering, Chinese Academy of Sciences. Alkalinity was measured by neutralising all the basic species taken into account in the alkalinity expression by formic acid mixed with a pH sensitive dye and determined with spectrophotometric method. For Fe analysis, 50 µL of concentrated HNO_3 was added to acidify the sample to pH ~1-2, and dissolved Fe was measured spectrophotometrically at 562 nm using ferrozine assay. pH was measured on board in a micro-sensors system (Unisense) that was polarized continuously for 5 days before use.

Quantification of dissolved gas concentrations

Samples for hydrogen and methane analyses of iddingsite-rich mud were prepared by making a slurry of the push core mud (5mL syringe subcores) and helium purged NaOH (2M) in 50 mL serum vials. A headspace of ultrahigh purity helium was introduced by displacement in each vial and was then vigorously shaken. After the samples were allowed to equilibrate under 4 °C for at least 12 h, headspaces were removed for concentration analysis by gas chromatography (GC), using a Thermo Fisher GC-1310 equipped with a pulsed discharge detector (PDD).

Determination of oxygen isotope compositions of carbonates

Analyses of oxygen isotope compositions of carbonates extracted from altered rocks were carried out from bulk rock powders at the Stable Isotope Laboratory, Third Institute of Oceanography, State Oceanic Administration, China. The $\delta^{18}O_{CaCO3}$ values were analysed using the stable isotope mass spectrometer (Thermo Delta V Advantages). The analytical accuracy of the $\delta^{18}O$ values was better than ±0.2 ‰. Oxygen isotope values are reported as standard δ-notation (in units of per mil, ‰), relative to the SMOW standard. They were calculated according to the following equation:

$$\delta^{18}O\ (‰) = [(^{18}O/^{16}O)_{sample} / (^{18}O/^{16}O)_{SMOW} - 1] \times 1000 \quad \text{Eq. S-1}$$

where $(^{18}O/^{16}O)_{SMOW}$ is the oxygen isotope ratio of SMOW.

DNA extraction and PCR amplification

Microbial genomic DNA of the samples was extracted with the PowerSoil DNA Isolation Kit (MoBio Laboratories, Carlsbad, CA, USA). The quality of extracted DNA was checked by 1 % agarose gel electrophoresis and spectrophotometry (optical density at 260 nm/280 nm ratio). All DNA was stored at –20 °C before further analysis. The V3-V4 hyper variable regions of the 16S rRNA gene were amplified by PCR for high-throughput sequencing. The V3-V4 region of 16S rRNA gene was amplified with the Bacteria primer set 338F (5′-ACTCCTACGGGAGGCAGCA-3′) and 806R (5′-GGACTACHVGGGTWTCTAAT-3′), and Archaea primer set Arch344F (5′-ACGGGGYGCAGCAGGCGCGA-3′) and Arch806R (5′-GGACTACVSGGGTATCTAAT-3′), respectively. The amplification procedure was as follows: 95 °C for 5 min, 25 cycles of 95 °C for 30 s, 55 °C for 30 s, and 72 °C for 40 s with a final extension of 72 °C for 10 min. The PCR products were separated by 1 % agarose gel electrophoresis and the about 460 bp fragments were purified by using Agencourt AMPure XP (Beckman Coulter, Inc., CA, USA).

Illumina sequencing and bioinformatics analysis

Sequencing was performed using Illumina Miseq PE300 sequencing platform (Illumina, Inc., CA, USA). Raw sequencing data were processed by Beijing Auwigene Tech, Ltd. (Beijing, China) using the pipeline tools QIIME (version v.1.8.0) and MOTHUR (version v.1.30.1). To retain only high-quality sequences for the downstream analysis, sequences that were less than 150 bp in length after quality trimming, contained one or more ambiguous base-calls (N), or had < 90 % quality scores > Q20 were eliminated. After

trimming, high-quality sequences were aligned to the Ribosomal Database Project (RDP) Multiclassifier tool, which is available from the RDP website. Reads obtained in the FASTA format were assigned to class levels with a 70 % confidence threshold. All of the aligned sequences were then clustered into operational taxonomical units (OTU) using QIIME (version v.1.8.0) at a 97 % similarity level. Before further analysis, singleton OTUs were removed using UPARSE (usearch v8.1. 1861). The taxonomic position of each OTU was automatically assigned based on Blast analysis in the QIIME software package. α-Diversity indices (rarefaction curves, Chao1, ACE, Shannon, Shannon evenness, and Simpson) in each library and taxa/divisions were also calculated using MOTHUR. Phylogenetic trees were constructed via the neighbor-joining method using the software MEGA (VERSION 6.06). The sequence reads have been deposited at the NCBI Short Read Archive (SRA) under the accessions SRR6292229 for the bacteria and SRR6292230 for the archaea.

Metagenomic analysis

Genomic DNA was extracted and purified from 10 g (wet weight) of sediment samples using the MOBIO PowerMax soil DNA isolation kit (MoBio Laboratories, Carlsbad, CA, USA). The quality of extracted DNA was checked by 1 % agarose gel electrophoresis and pectrophotometry (optical density at 260 nm/280 nm ratio). The extracted DNA sample was afterwards processed according to the genomic DNA sample preparation kit protocol (Illumina). Metagenome sequencing was performed on the platform Illumina Hiseq 3000.

Total sequence data obtained from the sample was 13.47 Gb (31, 530, 234 raw reads). Unassembled DNA sequences were annotated using the Metagenomics Rapid Annotation (MG-RAST) server (version 3.1), the reads were not assembled or filtered before submission for taxonomic and functional analyses (Meyer *et al*., 2008). The raw metagenomic sequence reads were aligned to the NCBI non-redundant (NR) database using BLASTX. After filtering the low quality reads following criteria: a quality score two s.d. smaller than the average, a length two s.d. smaller or larger than the average and ambiguous bases (Ns). The resulting 29,193,843 reads were used for genome assembly. The reads were assembled into contig using the MEGAHIT. Putative open reading frames (ORFs) were predicted using the software MetaGeneMark. The predicted genes obtained from the sample were combined and clustered using CD-HIT at 95 % identity and 90 % coverage length. The genes were further annotated by alignment using BLASTX against Kyoto Encyclopedia of Genes and Genomes (KEGG) Database. The information on metabolism pathway and KEGG Orthology (KO) was updated by retrieving the data from KEGG webserver. Representative metabolic pathways for the methanogenesis steps of samples were constructed from the KEGG database and contigs were compared with the database to detect key methanogenesis genes. The sequences have been deposited at the NCBI Sequence Read Archive (Whole Genome Submission) under BioProject ID PRJNA419272 with accession no. SRR6318720.

Supplementary Text

Origin of iddingsite

The term "iddingsite" has been used as a catchall phrase for the reddish-brown alteration products of olivine that form in an oxidising and fluid-rich environment. Besides olivine, reddish-brown iddingsite can also form as an alteration product of pyroxene. We infer that iddingsite at site M, N and P represents alteration of pyroxene (augite) rather than olivine based on: (1) unaltered rocks are primarily composed of augite and labradorite; (2) iddingsitization commonly occurs in the crack and rim of augite in partly altered rocks; and (3) iddingsite exhibits round morphologies similar to unaltered augite (Fig. S-2).

Post-precipitation of birnessite in the altered rocks

Transmitted microscopy images of thin sections show that birnessite is present in the altered rocks in the newly discovered mud volcano field. We suggest that those birnessite is post-precipitated after the formation of iddingsite, according to: (1) birnessite precipitated as veins filling in the interstice among iddingsite in altered rocks (Fig. 3b); and (2) no birnessite was observed to co-precipitate with iddingsite at the early stage of iddingsitization in partly altered rocks (Fig. 2d). We infer that high degree of iddingsitization in the highly altered rocks greatly increased the porosity of rocks and allowed the entrance of massive seawater that brought Mn^{2+} into the altered rocks. The formation of birnessite in the altered rocks might be similar to that of Mn oxides in Mn-rich crusts formed on the surface of ocean crusts and seamounts.

Diversity of microbial communities in the altered rocks

A total of 26950 of 16S rRNA gene sequences of bacteria and 47690 of 16S rRNA gene sequences of archaea from altered rocks

passed all quality control filters.

Represented bacterial phyla were *Proteobacteria* (61.34 %), *Chloroflexi* (14.34 %), *Firmicutes* (11.09 %), *Nitrospirae* (3.38 %). Within *Proteobacteria*, the γ-subdivision was the most dominant class and it represented 31.08 % of all bacterial 16S rRNA gene sequences. Numbers of OTUs obtained from samples were highly similar to Dehalogenimonas lykanthroporepellens belonged to the *Chloroflexi*, which were strictly anaerobic and used hydrogen as an electron donor. Many of sequences were similar to *Desulfonatronum spp*., *Desulfobacca spp*., *Desulfovibrio spp*., *Desulfonauticus spp*., *Desulfuromonas spp*., *Desulfomonile spp*., Desulfarculus spp., and *Desulfonatronobacter spp*. belonged to *Deltaproteobacteria*, which were closely related to sulfate-reducing coupled hydrogen oxidation. Members of the Firmicutes included two unique genera, *Desulfotomaculum* and *Desulfovirgula*, which were better known to use readily hydrogen for growth through sulfate reduction. The majority of *Nitrospirae* sequences were highly similar to *Thermodesulfovibrio hydrogeniphilus*, a thermophilic sulfate-reducer coupling utilisation of H_2 as an electron donor isolated from the geothermal underground mine and hot spring.

The archaeal communities were dominated by *Thaumarchaeota* (80.88 %) followed by *Euryarchaeota* (13.02 %) and *Crenarchaeota* (0.55 %). The majority of the *Euryarchaeot*a sequences were associated with the methanogens, including members of the family *Methanococcacea, Methanoregulaceae, Methanosaetaceae* and *Methanobacteriacea*. All these families including *Methanococcacea*, *Methanoregulacea*e, and *Methanobacteriacea* were obligately H_2-dependent, except for *Methanosaetaceae* that were acetate-utilising representatives. A number of sequences related to *Methanococcacea* were highly similar to *Methanococcus maripaludis*, which were better known to consume H_2 for growth. *Methanoregula spp*. belonged to members of *Methanoregulaceae*, which were isolated from the methanogenic digester sludge, were also detected. The genera *Methanosaeta* within *Methanosaetaceae* were considered to be active methanogens by oxidation acetate to produce methane.

Metagenomic analyses of the iddingsite-rich muds

Methanogenesis is catalysed exclusively by members of the Euryarchaeota, which are phylogenetically diverse in our samples (Fig. S-5). Methanogenic archaea could be classified into seven orders: M*ethanobacteriales, Methanococcales, Methanomicrobiales, Methanosarcinales, Methanocellales, Methanopyrales* and *Methanomassiliicoccales*.

H_2-CO_2-dependent methanogenesis is thought to be the main pathway for CH_4 production, which was found in all methanogenic orders with the exception of *Methanomassiliicoccales* in our samples. The *order Methanobacteriales, Methanococcales, Methanomicrobiales*, and *Methanopyrales* that were identified in iddingsite-rich muds are exclusively hydrogentrophic methanogens. The two genera *Methanosaeta* and *Methanosarcina* within *Methanosarcinales* were also detected, whereas those most closely related to *Methanosarcina* are considered to be facultative methanogens that can additionally use hydrogenotrophic and acetoclastic pathways of methanogenesis. The order *Methanocellales* more active under low hydrogen partial pressure is closely related to the orders *Methanosarcinales* and *Methanomicrobiale*s. However, substrate for methane production of the order *Methanocellales* is comparable with Methanomicrobiales that is hydrogenotrophic. In addition, Methylotrophic methanogens were also found in the orders of *Methanosarcinale*s and *Methanomassiliicoccales* that produce methane by reducing methanol with hydrogen as the electron donor.

Functional enzyme-encoding genes for the methanogenesis pathways were identified and annotated by the KEGG database in this study (Fig. S-6). For hydrogenotrophic methanogenesis, substrates of H_2/CO_2 to methane through a series of relevant enzymes, including formylmethanofuran dehydrogenase (fmd, EC: 1. 2. 7. 12), formylmethanofuran-tetrahydromethanopterin N-formyltransferase (ftr, EC: 2.3.1.101), methenyltetrahydromethanopterin cyclohydrolase (mch, EC: 3.5.4.27), methylenetetrahydromethanopterin dehydrogenase (mtd, EC: 1.5.98.1), coenzyme F420 hydrogenase (frh, EC: 1.12.98.1), and coenzyme F420-dependent N5, N10-methenyltetrahydromethanopterin reductase (mer, EC: 1.5.98.2). For acetoclastic methanogenesis, acetyl-CoA synthetase (acs, EC: 6.2.1.1), acetate kinase (ack, EC: 2.7.2.1) and phosphate acetyltransferase (pta, EC: 2.3.1.8) play a critical role in the conversion of acetate to methane. For methylotrophic pathway, the genes coding for the methanol-specific corrinoid proteins are essential for the conversion of methyl groups from methanol to methane. Moreover, the methyl-CoM is subsequently converted to methane through several key enzymes of tetrahydromethanopterin S-methyltransferase (mtr, EC: 2.1.1.86), methyl coenzyme M reductase (mcr, EC: 2.8.4.1) and heterodisulfide reductase (Hdr, EC: 1.8.98.1) at the final reaction steps.

Supplementary Tables

Table S-1 Location of the mud volcanoes and pockmarks

Site Name	Depth (m)	Latitude	Longitude
M	5500	10° 51.05′	141° 57.02′
N	6300	10° 53.37′	142° 13.56′
P	6669	10° 55.20′	141° 41.40′

Table S-2 Representative chemical compositions of iddingsite (Idd) and augite (Aug)[a] obtained by EPMA

Site Name	Aug-1	Aug-2	Aug-3	Idd-1	Idd-2	Idd-3	Idd-4	Idd-5	Idd-6	Idd-7	Idd-8	Idd-9	Idd-10
SiO_2	53.31	53.44	52.70	49.65	51.27	50.85	54.25	53.75	44.46	43.69	47.15	39.76	41.78
TiO_2	0.35	0.42	0.49	bd	bd	bd	0.03	bd	bd	bd	bd	0.01	bd
Al_2O_3	2.82	2.76	2.87	0.17	0.23	0.10	1.82	1.44	0.31	0.23	0.23	0.89	0.86
Cr_2O_3	0.73	0.73	0.21	0.02	0.05	0.01	0.13	0.22	0.04	0.06	0.01	0.01	Bd
FeO	5.00	4.93	6.45	28.14	28.38	28.39	26.44	27.01	31.38	22.13	27.61	31.05	28.26
NiO	Bd	bd	bd	bd	0.05	bd	Bd	0.03	0.06	0.02	0.02	bd	bd
MnO	0.12	0.10	0.20	0.06	0.14	0.20	0.21	0.19	0.17	0.24	0.44	0.48	0.49
MgO	17.12	17.28	16.25	3.67	3.64	3.75	4.08	3.58	3.09	2.69	3.36	2.69	2.99
CaO	20.23	20.13	19.84	0.69	0.68	0.61	0.75	0.44	0.21	0.06	0.08	0.24	0.14
K_2O	bd	bd	bd	2.79	2.83	2.78	1.93	2.10	2.78	2.77	3.59	3.00	3.52
Na_2O	0.21	0.24	0.23	0.14	0.22	0.19	0.57	0.77	1.59	1.00	1.30	1.06	1.09
Total	99.88	100.05	99.24	85.33	87.48	86.87	90.20	89.54	84.06	72.89	83.79	79.18	79.13
Fe^{2+}/Fe^{3+}	10000	10000	10000	0.000	0.000	0.000	0.000	0.000	0.000	0.000	0.000	0.000	0.000
FeO	5.00	4.93	6.45	0.00	0.00	0.00	0.00	0.00	0.00	0.00	0.00	0.00	0.00
Fe_2O_3	0.00	0.00	0.00	31.27	31.54	31.55	29.38	30.02	34.88	24.60	30.68	34.50	31.40
Corrected total	99.88	100.05	99.24	88.46	90.64	90.03	93.14	92.55	87.55	75.35	86.86	82.64	82.27
Si	1.95	1.95	1.95	0.83	0.85	0.85	0.90	0.89	0.74	0.73	0.78	0.66	0.70
Ti	0.01	0.01	0.01	0.00	0.00	0.00	0.00	0.00	0.00	0.00	0.00	0.00	0.00
Al	0.12	0.12	0.13	0.00	0.00	0.00	0.04	0.03	0.01	0.00	0.00	0.02	0.02
Cr	0.02	0.02	0.00	0.00	0.00	0.00	0.00	0.00	0.00	0.00	0.00	0.00	0.00
Fe^{2+}	0.15	0.15	0.20	0.00	0.00	0.00	0.00	0.00	0.00	0.00	0.00	0.00	0.00
Fe^{3+}	0.00	0.00	0.00	0.39	0.40	0.40	0.37	0.38	0.44	0.31	0.38	0.43	0.39
Ni	0.00	0.00	0.00	0.00	0.00	0.00	0.00	0.00	0.00	0.00	0.00	0.00	0.00
Mn	0.00	0.00	0.01	0.00	0.00	0.00	0.00	0.00	0.00	0.00	0.01	0.01	0.01
Mg	0.93	0.94	0.90	0.09	0.09	0.09	0.10	0.09	0.08	0.07	0.08	0.07	0.07
Ca	0.79	0.79	0.79	0.01	0.01	0.01	0.01	0.01	0.00	0.00	0.00	0.00	0.00
K	0.00	0.00	0.00	0.06	0.06	0.06	0.04	0.04	0.06	0.06	0.08	0.06	0.07
Na	0.02	0.02	0.02	0.00	0.01	0.01	0.02	0.02	0.05	0.03	0.04	0.03	0.04
Sum octahedral	2.00	2.00	2.00	0.56	0.57	0.57	0.58	0.58	0.64	0.48	0.60	0.63	0.60
Sum	2.00	2.00	2.00	0.83	0.85	0.85	0.90	0.89	0.74	0.73	0.78	0.66	0.70

tetrahedral Total cations	4.00	4.00	4.00	1.39	1.42	1.42	1.49	1.47	1.38	1.20	1.38	1.29	1.30

bd: below detection limits.

[a]: Augite data reduced using four cations atoms *per* formula unit.

Table S-3 Estimated temperatures for the alteration reaction.

Sample ID	$\Delta^{18}O$[a] (‰SMOW)	Temperature[b] (°C; -4‰ fluid)
JL114-G02	12.4	103
JL114-G06	13.4	93
JL115-G03	9.8	130

[a] Oxygen isotope composition of carbonates extracted from altered rocks.

[b] The temperature was estimated by the algebraic equation described previously:

$1000\ln\alpha = 2.78\times(10^6T^{-2})-3.39$

where the fractionation factor $\alpha = (^{18}O/^{16}O)CaCO_3 / (^{18}O/^{16}O)$fluid, and we assumed equilibrium with ^{18}O-depleted fluids (-4 ‰, SMOW) resulted from low-temperature reaction of seawater with basalt (Alt *et al*., 1986).

Table S-4 Analyses of whole-rock major element compositions of altered, unaltered and partly altered rocks.

Sample#	Sample type	Loss on ignition	Al_2O_3	CaO	CO_2	Fe_2O_3	K_2O	MgO	MnO	Na_2O	P_2O_5	SiO_2	TiO_2
JL114-G02	Altered rock	15.70 %	0.26 %	1.70 %	5.00%	11.40 %	0.55 %	2.20 %	48.42 %	5.13 %	0.24 %	8.07 %	bd
JL114-G06		19.56 %	5.39 %	2.82 %	bd	21.20 %	0.75 %	3.05 %	20.62 %	2.42 %	0.54 %	20.56 %	0.93 %
JL114-G12		14.59 %	0.57 %	0.71 %	bd	21.47 %	1.29 %	3.97 %	27.62 %	2.34 %	0.00 %	26.90 %	bd
JL114-G14		17.76 %	2.09 %	1.79 %	5.20%	13.45 %	0.83 %	3.37 %	39.01 %	3.34 %	0.36 %	10.75 %	0.37 %
JL115-G01		16.56 %	2.36 %	1.59 %	bd	22.96 %	1.14 %	3.55 %	23.16 %	2.23 %	0.30 %	24.83 %	0.41 %
JL115-G03		12.42 %	0.81 %	1.01 %	bd	14.62 %	1.49 %	4.06 %	41.47 %	2.35 %	0.08 %	20.60 %	0.05 %
JL115-G06		15.05 %	2.07 %	1.20 %	bd	21.55 %	1.39 %	3.74 %	21.25 %	2.38 %	0.18 %	29.90 %	0.30 %
JL115-G08		19.04 %	2.95 %	2.21 %	bd	22.70 %	0.86 %	2.90 %	27.54 %	2.06 %	0.55 %	16.97 %	0.71 %
JL115-G09		15.79 %	1.03 %	0.92 %	bd	20.21 %	1.49 %	3.91 %	26.23 %	2.13 %	0.11 %	27.51 %	0.00 %
JL115-G14		16.62 %	2.74 %	1.82 %	bd	2.93 %	0.82 %	3.57 %	48.27 %	11.84 %	0.15 %	10.03 %	0.14 %
JL116-G01	Unaltered rock	1.85 %	12.08 %	14.06 %	bd	16.84 %	0.38 %	5.97 %	0.54 %	2.69 %	bd	43.67 %	1.75 %
JL116-G02		1.67 %	13.80 %	14.85 %	bd	14.15 %	0.25 %	5.75 %	0.30 %	2.93 %	bd	44.49 %	1.63 %
JL116-G03		1.58 %	13.48 %	14.88 %	bd	15.13 %	0.24 %	5.61 %	0.24 %	2.77 %	0.16 %	44.03 %	1.61 %
JL116-G04		1.69 %	13.23 %	15.09 %	bd	14.08 %	0.28 %	5.28 %	0.24 %	3.04 %	0.17 %	44.91 %	1.74 %
JL116-G10-1	Partly altered rock	11.68 %	10.13 %	2.75 %	bd	14.06 %	1.70 %	5.87 %	2.29 %	3.66 %	0.32 %	45.50 %	0.81 %
JL116-G10-2		11.56 %	11.49 %	2.80 %	bd	11.15 %	1.79 %	5.75 %	5.15 %	3.68 %	0.32 %	44.01 %	0.84 %
JL116-G10-3		11.68 %	10.64 %	2.92 %	bd	13.38 %	1.69 %	5.64 %	2.41 %	3.66 %	0.31 %	45.70 %	0.75 %

bd: below detection limits

Table S-5 Chemical characterization of pore water samples

Location	pH	Alk	Mg (mmol/kg)	Ca (mmol/kg)	Na (mmol/kg)	Cl (mmol/kg)	SO_4 (mmol/kg)	CH_4 (nmol/L)	H_2 (nmol/L)	Ref.
Reference site[a]	/	1.9-2.9	56.0-70.2	10.6-14.1	490.8-601.4	566.5-589.2	26.6-28.0	90-200	200-3000	This work
Site M[b]	7.2-7.5	3.0-4.1	50.0-53.4	10.1-10.7	447.5-478.2	506.4-549.9	29.5-32.5	700-1800	4700-40900	This work
Serpentinite mud volcano	8.1-12.5	2.3-68.7	0-44	0.3-74.8	220-688	260-546	6.9-46	/	/	Mottl *et al.*, 2004; Hulme *et al.*, 2010

CH_4 and H_2 values are a minimum because samples were not run onboard, but after two weeks in cold storage. Gases were probably lost during sampling and/or diffusively during storage.
Reference site[a]: TS03 GT01
Site M[b]: JL114 & 115

Table S-6 Hits numbers of genes involved in the relevant methanogenesis pathways in mud samples

Enzyme	Enzyme	KO pathway	Hits
Fmd	EC: 1.2.7.12	K00200	218
		K00201	178
		K00202	64
		K00203	12
		K11261	16
Ftr	EC:2.3.1.101	K00672	76
Mch	EC:3.5.4.27	K01499	86
Mtd	EC: 1.5.98.1	K00319	16
Mer	EC: 1.5.98.2	K00320	86
Frh	EC:1.12.98.1	K00441	104
Mcr	EC:2.8.4.1	K00399	72
Hdr	EC:1.8.98.1	K03388	2
		K03389	14
		K03390	4
Acs	EC:6.2.1.1	K01895	82
Ack	EC:2.7.2.1	K00925	398
Pta	EC:2.3.1.8	K00625	274
Cdh	EC:2.3.1.-	K00193	72
Mta	EC:2.1.1.246	K14080	78
Mtr	EC:2.1.1.86	K00577	120

Supplementary Figures

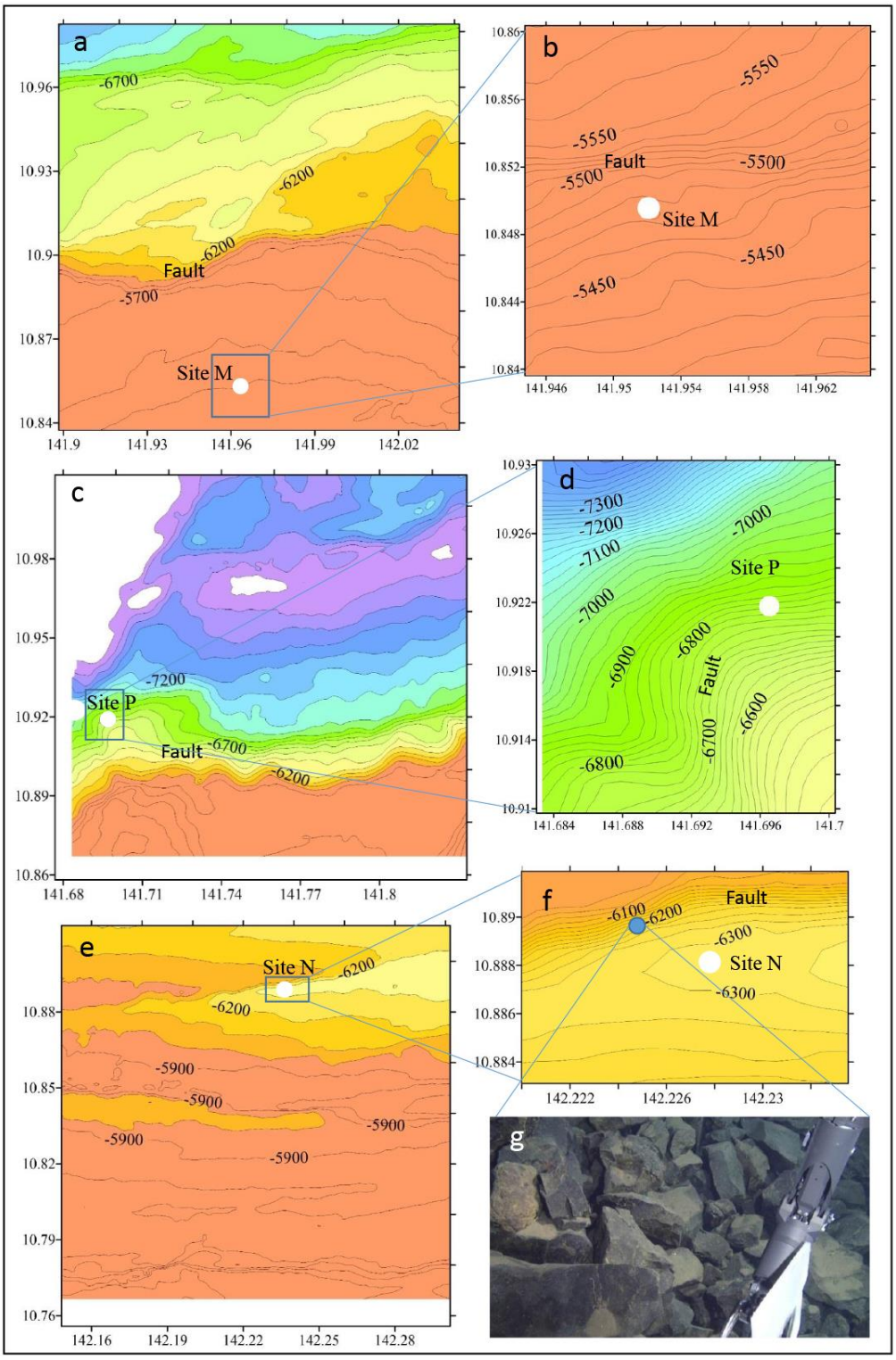

Figure S-1 Bathymetric maps showing that the sites M, P, N are closely related to bending-related faults and associated fracture zones. **(a)** Bathymetric map of the area nearby site M. **(b)** Enlargement of box in (a). **(c)** Bathymetric map of the area nearby site P. **(d)** Enlargement of box in (c). **(e)** Bathymetric map of the area nearby site N. **(f)** Enlargement of box in (e). **(g)** A fracture zone (blue dot in (f)) observed during *Jiaolong* dive in the vicinity of site N showing strong tectonic deformation.

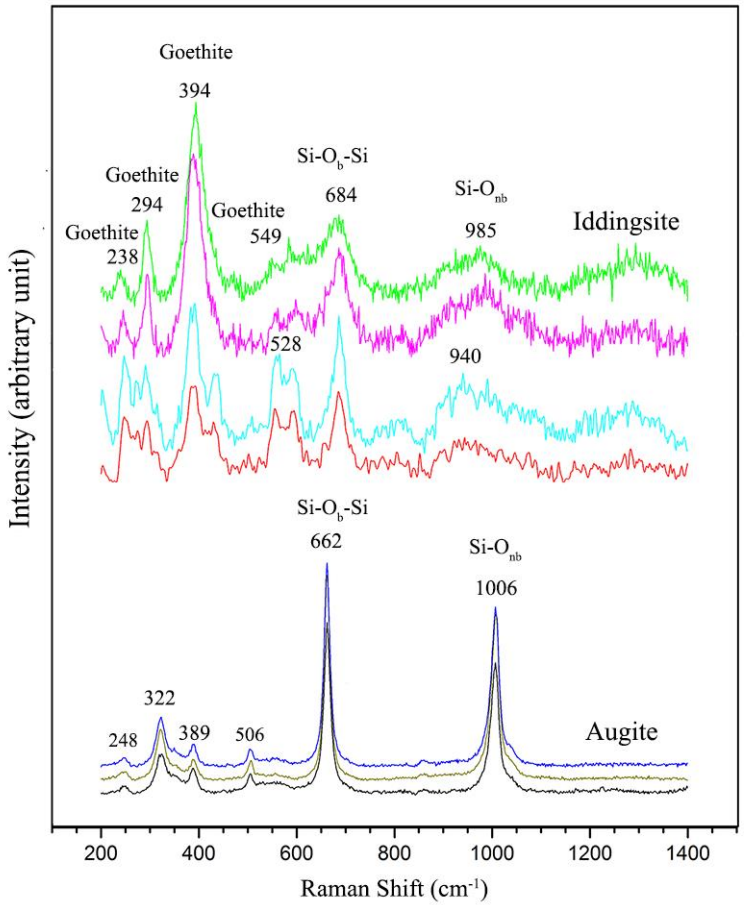

Figure S-2 Comparisons of representative Raman spectra from the iddingsite and the host augite. The spectrum of augite has a strong peak in the Si-O_b-Si stretching vibrational region (O_b = bridging oxygen) at 662 cm^{-1} and another in the Si-O_{nb} stretching vibrational region (O_{nb} = nonbridging oxygen) at 1006 cm-1. The spectrum of iddingsite is characterised by a peak near 684 cm-1, which can be attributed to the presence of Si-O_b-Si linkages in the structure. A weaker feature is located in the 850–1150 cm^{-1} region where Si-O_{nb} peaks occur, centered at near 940 and 985 cm^{-1}. The peaks at 394, 294, 238, 549 cm^{-1} are assigned to goethite. Changes in relative peak intensities and peak shifts of iddingsite indicate a mixture of phases and variable compositions.

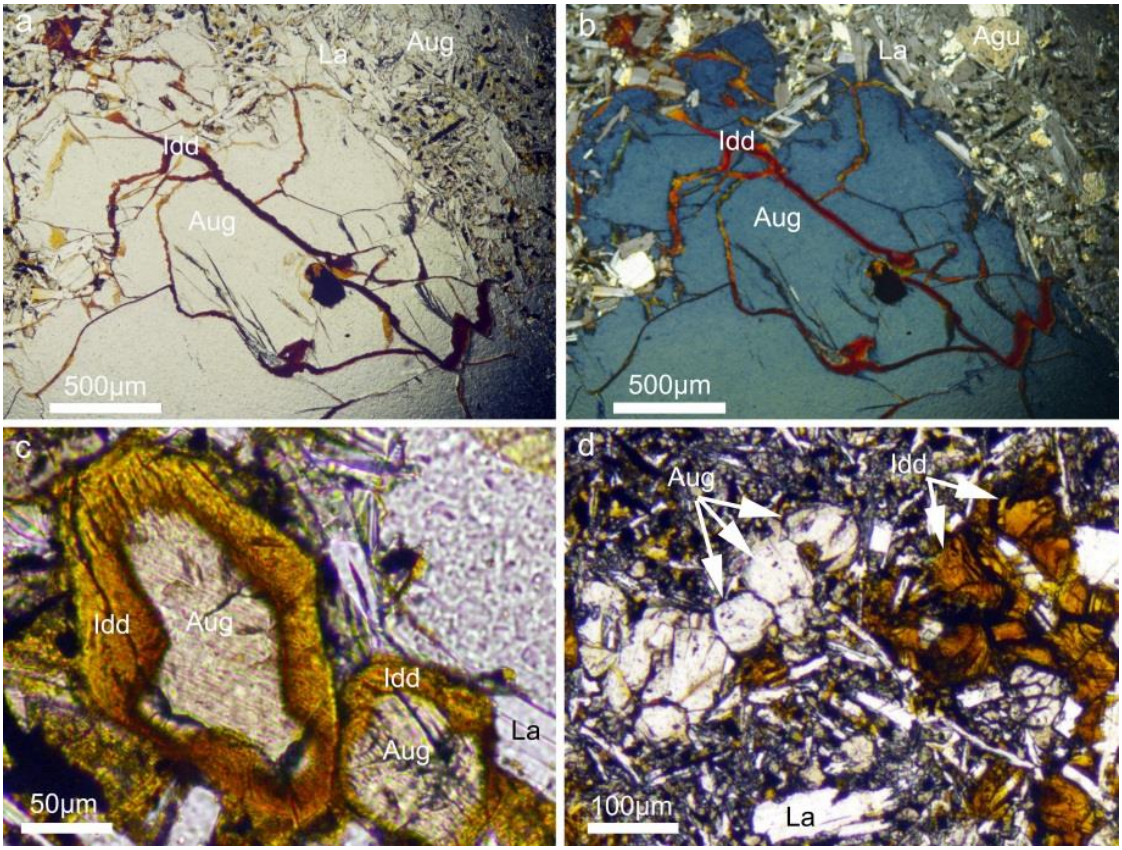

Figure S-3 Photomicrograph showing iddingsite derived from the alteration of augite in the partly altered basement rock (#JL116-Rock-2). **(a)** Image in plane polarised light showing that iddingsite forms along cracks of augite. **(b)** Image of the same area in (a) in perpendicular polarised light**. (c)** Image in plane polarised light showing aguite with alteration rim of reddish iddingsite. **(d)** Image in plane polarised light showing that iddingsite exhibits round morphologies similar to unaltered augite.

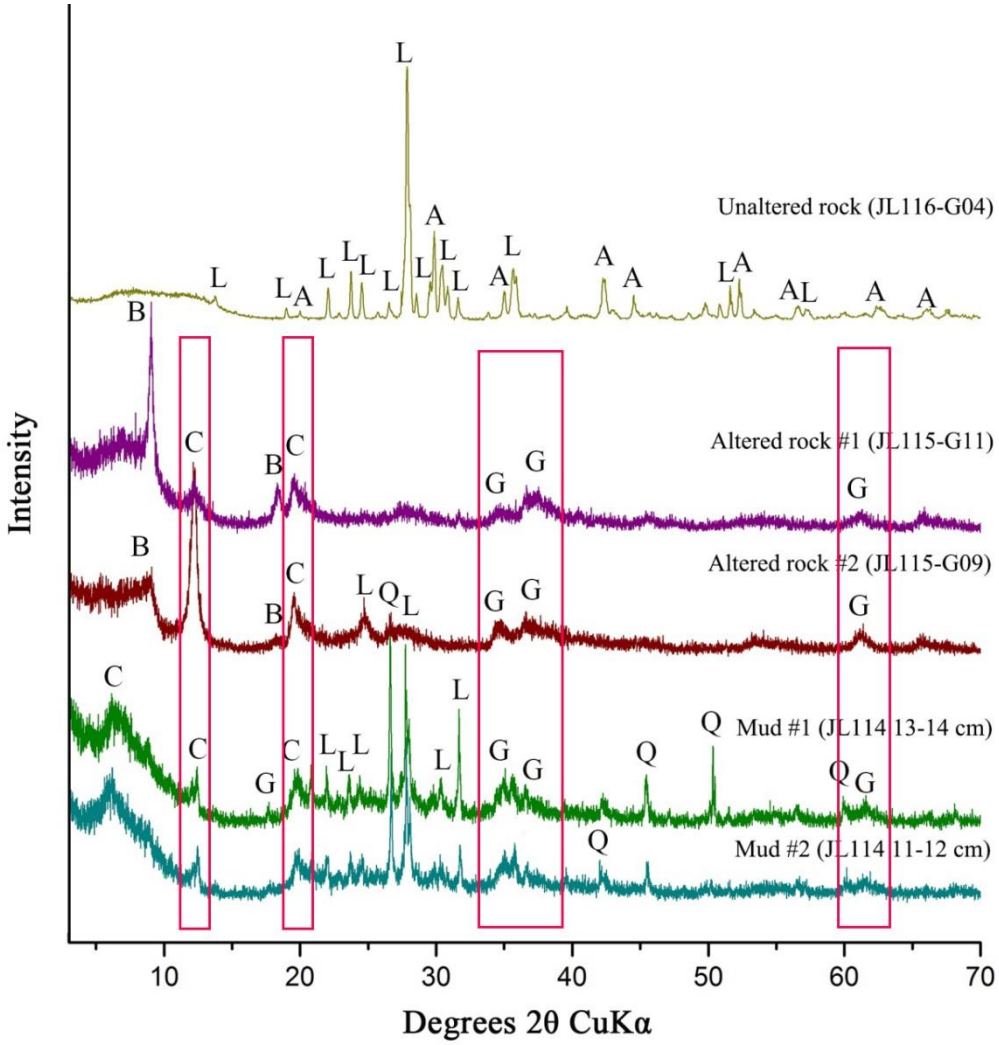

Figure S-4 XRD patterns of unaltered rocks, altered rocks and muds in the study area. Altered rocks and muds contain iddingsite that consist of peaks of goethite and clinochlore (clay), whereas unaltered rocks are composed of augite and labradorite. The peaks of quartz in mud are probably derived from pelagic sediments containing biogenic silica. A, augite; B, birnessite; C, clinochlore; G, goethite; L, labradorite, Q, quartz.

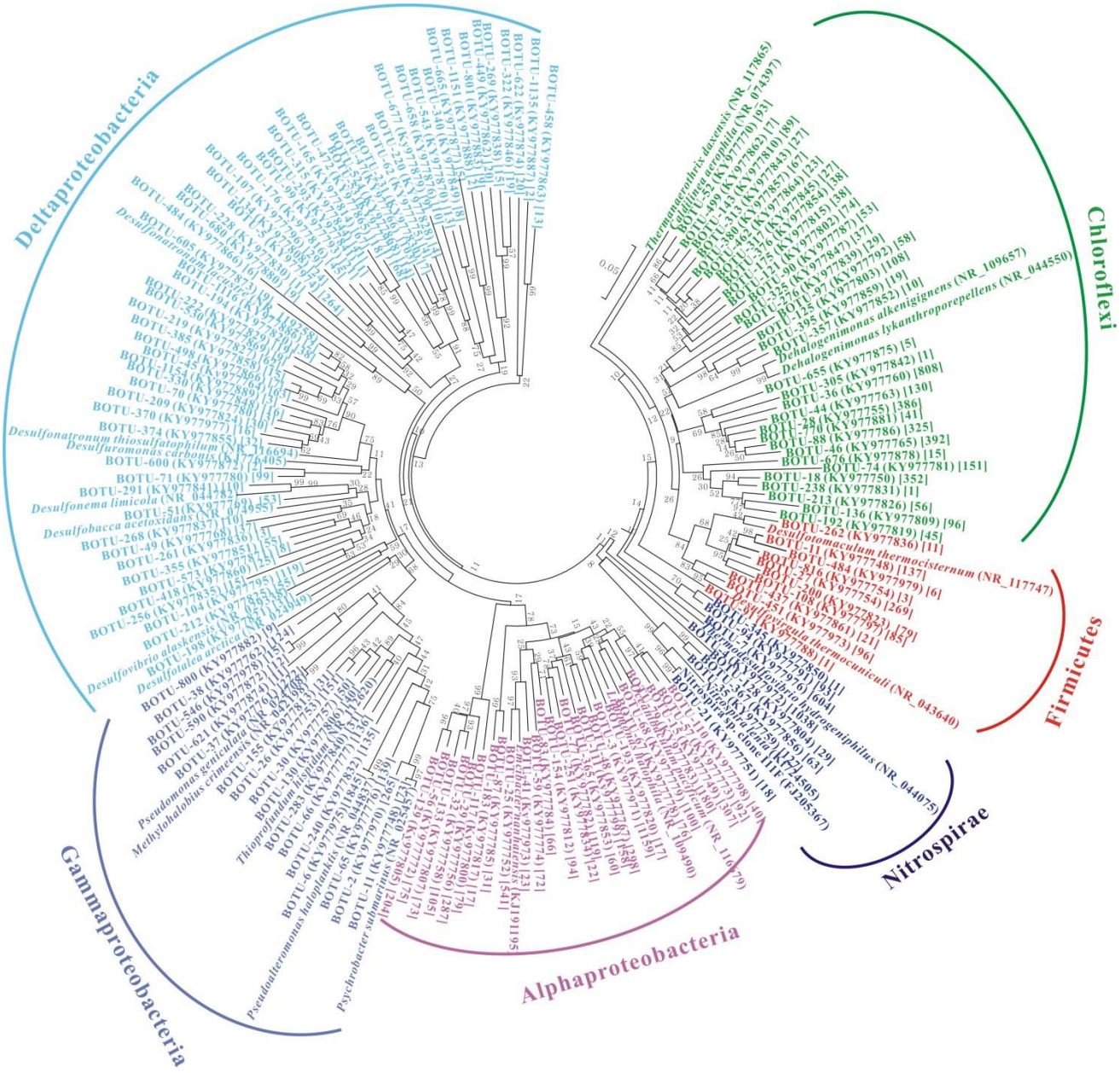

Figure S-5 Phylogenetic trees showing positions of Bacterial 16S rRNA gene sequence groups recovered from altered basement rocks. The tree is based on the neighbour-joining algorithm with bootstrap resampling (1000 times). Gene sequences from this study are denoted as BOTU and in bold type face. Values in brackets refer to the number of times particular bacterial phylotypes were recovered. The scale bar corresponds to 0.05 substitutions per nucleotide position.

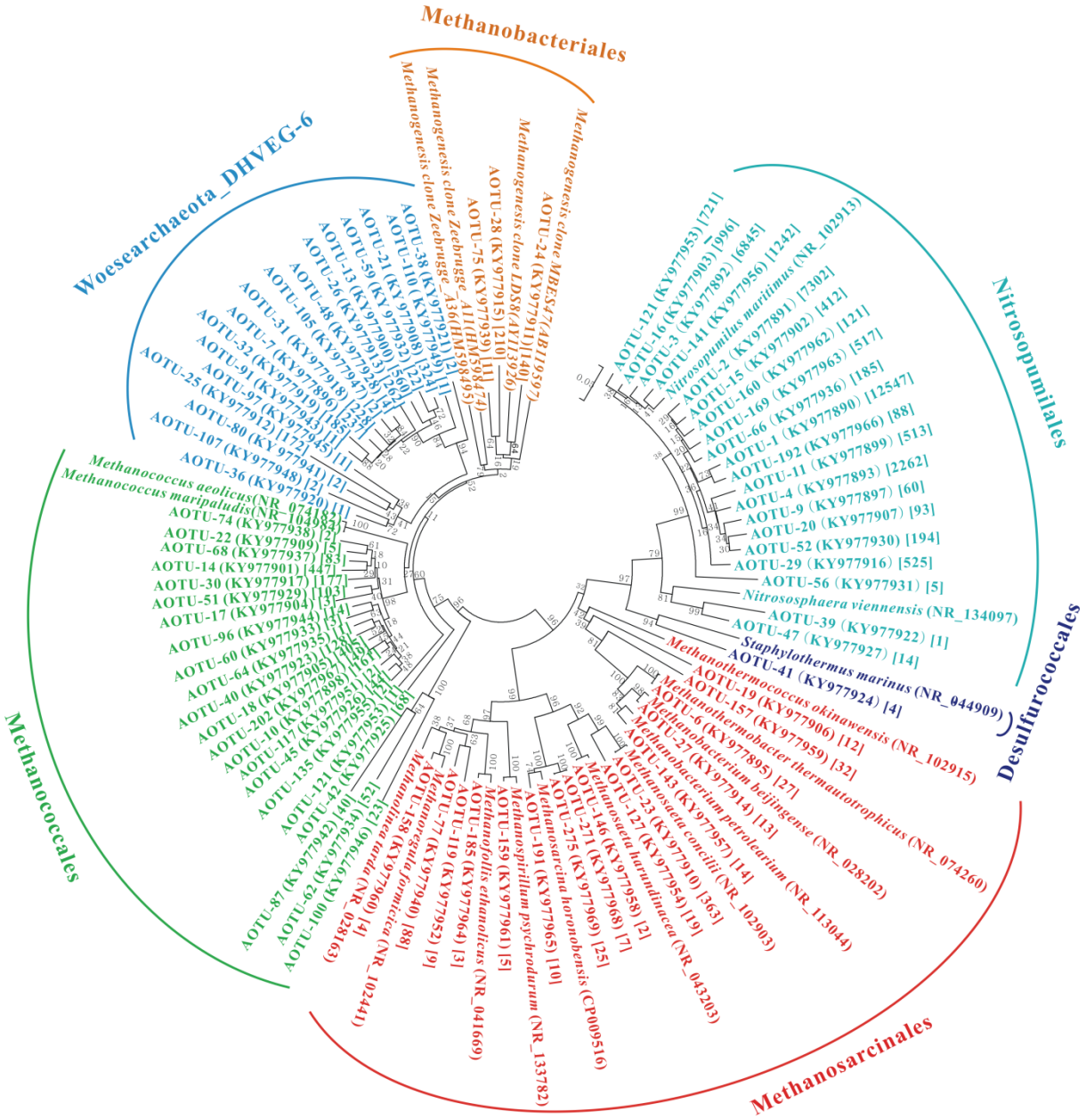

Figure S-6 Phylogenetic trees showing positions of Archaea 16S rRNA gene sequence groups recovered from altered basement rocks. The tree is based on the neighbour-joining algorithm with bootstrap resampling (1000 times). Gene sequences from this study are denoted as AOTU and in bold type face. Values in brackets refer to the number of times particular archaeal phylotypes were recovered. The scale bar corresponds to 0.05 substitutions per nucleotide position.

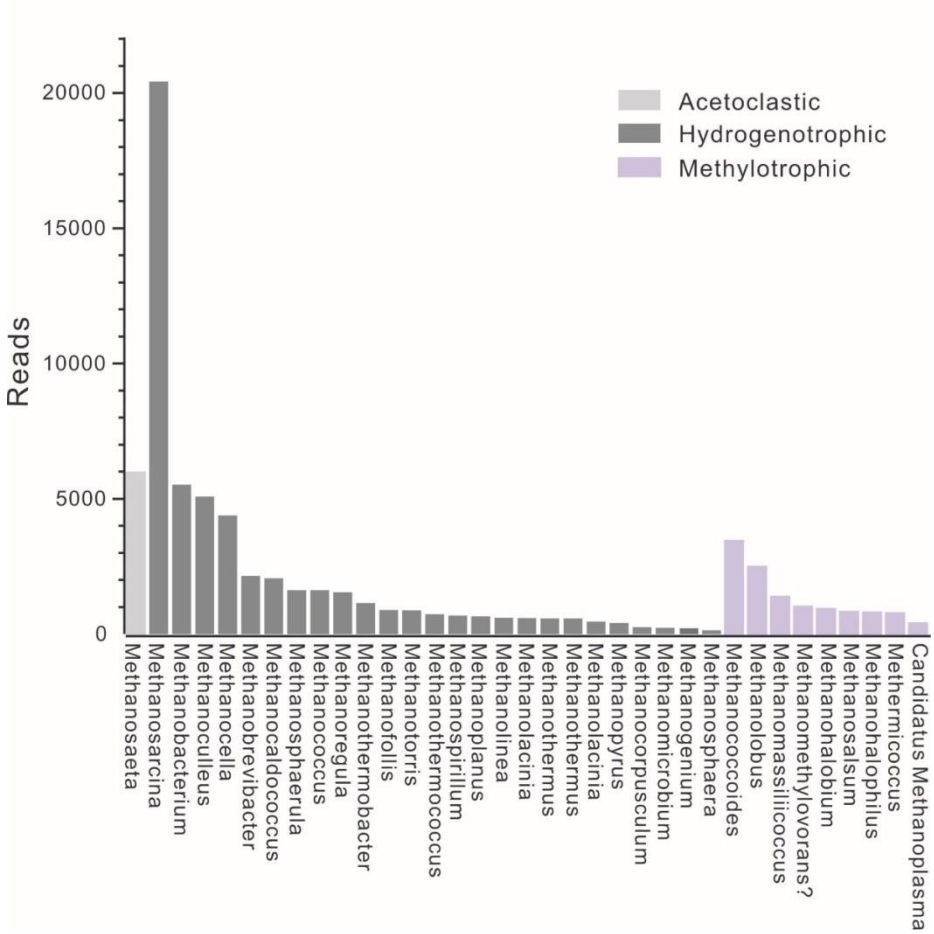

Figure S-7 Key genera involved in methanogenesis pathway in mud samples.

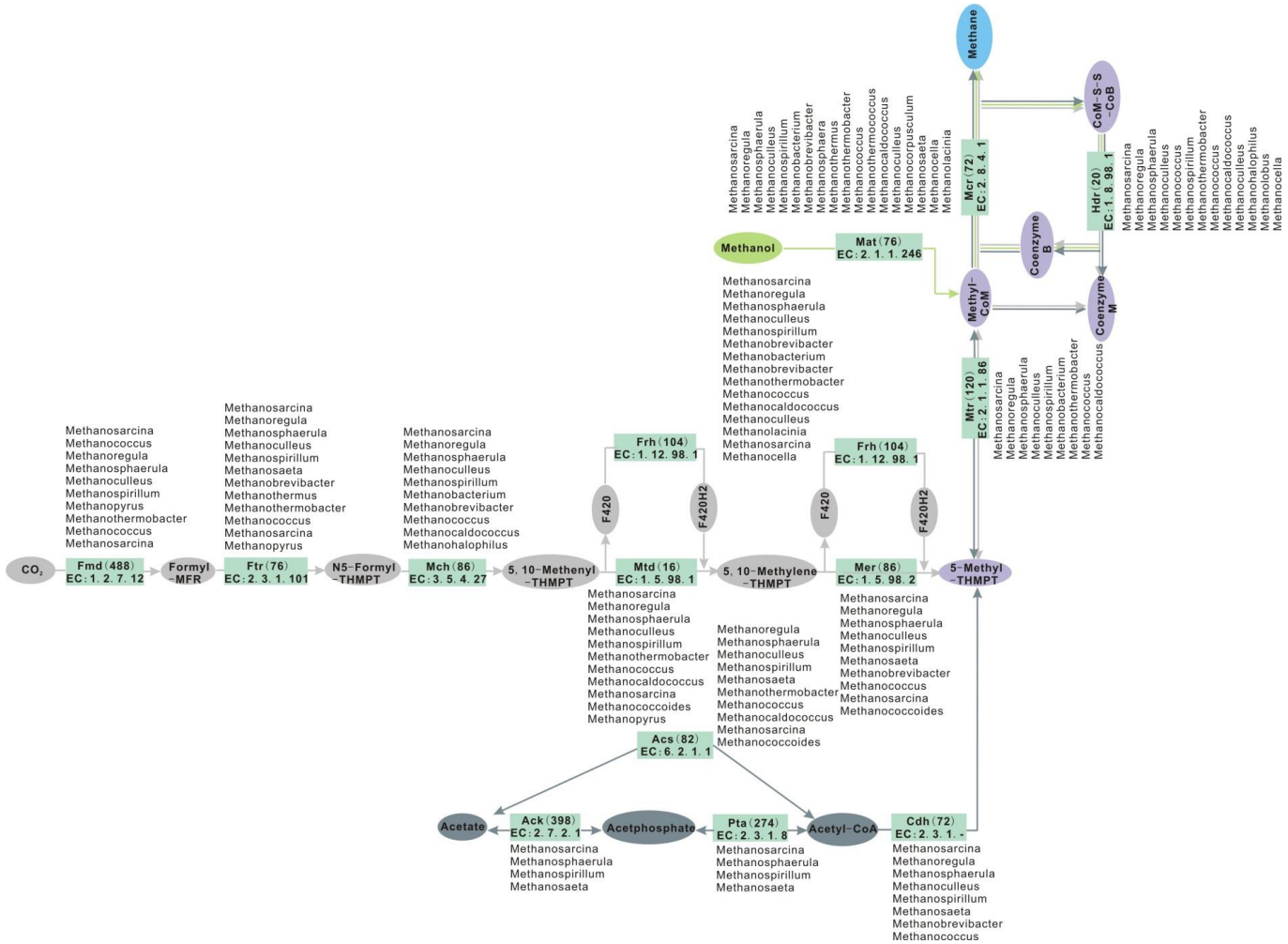

Figure S-8 Methanogenesis pathways predicted in mud samples based on the KEGG analysis.

Supplementary Video

Supplementary Video S-1 is available for download at http://www.geochemicalperspectivesletters.org/article1916.

Video S-1 Fluid discharge points and pockmarks observed in the southern Mariana trench during HOV Jiaolong dives.

Supplementary Information References

Alt, J.C., Muehlenbachs, K., Honnorez, J. (1986) An oxygen isotopic profile through the upper kilometer of the oceanic crust, DSDP Hole 504B. *Earth and Planetary Science Letters* 80, 217-229.

Mottl M.J., Wheat C. G., Fryer P., Gharib J., Martin J. B. (2004) Chemistry of springs across the Mariana forearc shows progressive devolatilization of the subducting plate. *Geochimica et Cosmochimica Acta* 68, 4915-4933.

Hulme S.M., Wheat C. G., Fryer P., Mottl M. J. (2010) Pore water chemistry of the Mariana serpentinite mud volcanoes: A window to the seismogenic zone. *Geochemistry, Geophysics, Geosystems* 11, 1.